

Learning Structure via Consensus for Face Segmentation and Parsing

Iacopo Masi Joe Mathai Wael AbdAlmageed
 USC Information Sciences Institute, Marina del Rey, CA, USA
 {iacopo, jmathai, wamageed}@isi.edu

Abstract

Face segmentation is the task of densely labeling pixels on the face according to their semantics. While current methods place an emphasis on developing sophisticated architectures, use conditional random fields for smoothness, or rather employ adversarial training, we follow an alternative path towards robust face segmentation and parsing. Occlusions, along with other parts of the face, have a proper structure that needs to be propagated in the model during training. Unlike state-of-the-art methods that treat face segmentation as an independent pixel prediction problem, we argue instead that it should hold highly correlated outputs within the same object pixels. We thereby offer a novel learning mechanism to enforce structure in the prediction via consensus, guided by a robust loss function that forces pixel objects to be consistent with each other. Our face parser is trained by transferring knowledge from another model, yet it encourages spatial consistency while fitting the labels. Different than current practice, our method enjoys pixel-wise predictions, yet paves the way for fewer artifacts, less sparse masks, and spatially coherent outputs.

1. Introduction

¹ The book [of Nature] is written in mathematical language, and the symbols are triangles, circles and other geometrical figures, without whose help it is impossible to comprehend a single word of it; without which one wanders in vain through a dark labyrinth.

Galileo Galilei, 1623 [16]

Face segmentation and parsing are invaluable tools since their output masks can enable next-generation face analysis tools, advanced face swapping [31, 49, 48], more complex face editing applications [62], and face completion [37, 35, 46]. Segmenting and parsing a face is strongly related to generic semantic segmentation [42, 36, 54, 27, 38, 11, 12] since it involves the task of densely predicting conditioned class probabilities for each pixel in the input image according to pixel semantics. Although the two share the

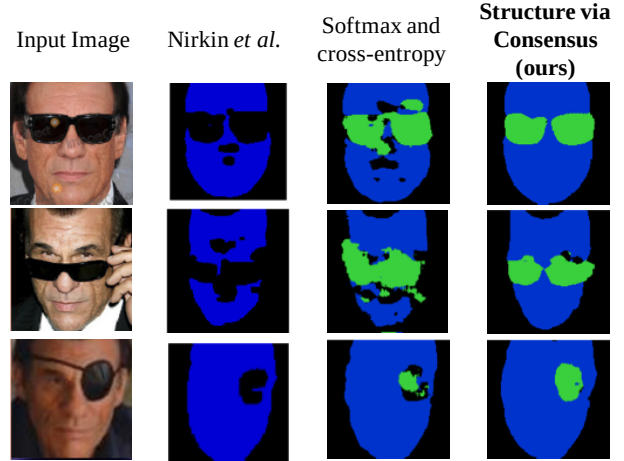


Figure 1: Structure via Consensus. From left to right: the input image; result by [49]; our model with softmax+cross-entropy; our proposed method. Previous methods predict only face (blue) vs. background (black), while ours yields separate predictions for occlusions (green) and background (black). Our loss enforces smoothness over objects covering the face via consensus constraint. Unlike state-of-the-art face parsing and segmentation methods [58, 49] that rely on *independent* pixel-wise softmax+cross-entropy loss—heavily used in generic semantic segmentation [42, 36, 54, 27, 38, 11, 12]—our learning is penalized for returning sparse, independent predictions through a novel formulation. This results in much more robust and solid occlusion detection and better generalization to unseen occlusions.

same methodology, face parsing is different than scene object segmentation since faces are already roughly scale and translation invariant, after a face detection step, and a plethora of methods has been developed towards solving the face parsing task [29, 40, 41, 39, 64, 51].

While state-of-the-art methods emphasize developing sophisticated architectures (e.g., two-stage networks with recurrent models [40]) or a complex face augmenter to simulate occlusions [49], or rather employ adversarial training [51], we take an alternative path towards robust face segmentation and parsing. Our method builds on an important observation related to the assumption of the *independent*

dence of pixel-wise predictions. Despite the significance of the aforementioned tasks, current methods overlook the regular structure present in nature and simply optimize for a cost that does not explicitly back-propagate any smoothness into the network parameters. This issue is particularly important for objects and faces, which have a well-defined and continuous (non-sparse) structure.

Fig. 1 shows the advantage of the proposed method on a few samples drawn from the validation set tested on unseen subjects. While publicly available state-of-the-art models [49] perform face segmentation, they do so with very sparse and noncontinuous predictions and by modeling two classes only (face, non-face). In contrast, by virtue of our method, we can separate occlusions from background, and more importantly, arrive at much more stable predictions that are hard to attain with a pixel-wise loss.

As also noted by [30, 25], training a network with pixel-wise softmax and cross-entropy for structured prediction makes the strong and too-simplistic assumption that pixel predictions are independent and identically distributed (i.i.d.). We take inspiration from the Gestalt laws [33]—particularly the ones of proximity (close pixels shall be perceived as a group), closure (pixels shall be grouped into complete figures), good continuation (objects often minimize discontinuity)—and in response to the previous too-simplistic assumption, we make the following contributions which propose: (1) factorizing out occlusions by means of the difference between the complete face shape, attained through a strong prior robustly computed via 3D projections [8, 45], and the output of a preexistent yet error-prone face segmentation network; (2) leveraging the connected components of the objects factorized before, using them as constraints to formulate a new loss function that still performs dense classification, yet enforces structure in the network by consensus learning; (3) finally showing that our approach is a generic tool for face parsing, thereby reporting state-of-the-art results in face parsing benchmarks [7, 29]. As an additional contribution, we will release our models and the related code.

The remainder of this paper is organized as follows. Section 2 discusses related work, Section 3 explains our method, Section 4 reports the experimental evaluation, and Section 5 abstracts our findings along with future work.

2. Related Work

Face segmentation. Recent work on face segmentation used a two-stream network [58] to predict a pixel-wise face segmentation mask. The system is fully supervised using pixel-wise segmentation masks obtained by preexisting data sets [23] or by additional semiautomatic manual efforts. Notably, [58] is trained with pixel-wise softmax+cross-entropy, and in order to enforce regularization in the predicted mask, the method uses a conditional random field

(CRF) as a post-processing step. Importantly, CRFs have been already used in generic object segmentation and expressed as recurrent layers [74]. Adversarial learning has been used too for segmentation in [43]. Unlike all these methods, ours presents key differences in the way smoothness is propagated in the network.

Similar to [58], Nirkin *et al.* [49] trained a simple fully convolutional net (FCN [42]) for binary face segmentation using a semi-supervised tool to support manual segmentation of faces in videos; in our method we transfer knowledge from the weights of [49], yet we demonstrate that by using our method we can learn from their mistakes and improve the model. Finally, Wang *et al.* [66] exploited temporal constraints and recurrent models for face parsing and segmentation in video sequences.

Semantic segmentation. Generic semantic segmentation has been an interesting topic in computer vision for a long time—starting with the seminal work using CRFs [6, 63] and graph cut [4, 5]. CRFs impose consistency across pixels, assessing different affinity measures and solving the optimization through a message-passing algorithm [57]. They have been successfully and widely used in face parsing applications also [29, 41]. Recently, they began to be used as a post-processing step [58, 41, 11] with convolutional networks and later on expressed as recurrent neural networks [74]. Super-pixels have also been employed to ease the segmentation process [15, 29], though recently, the field was revolutionized with end-to-end training of FCNs, [42] optimized simply by extending a classification loss [34] to each pixel *independently*. After [42], there has been extensive progress in deep semantic segmentation—mainly improving convolution to allow for wider receptive fields with its atrous (dilated) version [70, 71], different spatial pooling mechanisms, or more sophisticated architectures [36, 54, 27, 38, 11, 12].

Structure modeling. Modeling structure in computer vision dates back to perceptual organization [47, 59] and to the more general idea of describing objects with a few parts, advocating for frugality [3] in the shape description. Lately, with modern deep-learning, in addition to the aforementioned CRF formulation, all those concepts have faded away in the community—with some exceptions [65, 30]—and instead adversarial training [43, 24, 55, 25] has been used to impose structure in the prediction forcing the output distribution to match the distribution of ground-truth annotations. In doing so, the model is forced to produce output that is indistinguishable from the annotated mask, yielding eventually less sparse outputs. This introduces additional parameters to the training in the form of a discriminator that is learned by solving a usually difficult minimax game [19]. Other attempts incorporate boundary cues in the training process [1, 9] or pixel-wise affinity [2]. For an in-depth discussion on structured prediction, we refer to [50].

3. Face Parsing with Consensus Learning

Our objective is to robustly learn a nonlinear function ϕ parametrized by the weights of a convolutional neural network that maps pixel image intensities $\mathbf{I} \in \mathbb{R}^{3 \times H \times W}$ to a mask that represents per-pixel semantic label probabilities of the face $\mathbf{y} \in \mathbb{R}^{K \times H \times W}$. More formally, we aim to optimize $\phi(\mathbf{I})$ so that it maps $\phi: \mathbb{R}^{3 \times H \times W} \rightarrow \mathbb{R}^{K \times H \times W}$ where K is the number of classes considered in our problem. Importantly, in the learning of $\phi(\cdot)$, while we minimize the expected cost across the training set, we need to enforce a mechanism that incorporates structure through smoothness. At test-time, like current practice, we obtain a final, hard-prediction as $\mathbf{y}' \doteq \arg \max_k \phi(\mathbf{I})$ and $\mathbf{y}' \in \mathbb{R}^{1 \times H \times W}$.

The following sections discuss how to obtain some external constraints for enforcing smoothness during the training, though later on we show that our method can be easily employed for the generic face parsing task. We do so by means of transferring knowledge from an existing network and using a strong prior given by 3D face projection to factorize out occluding blobs (Section 3.1). Those blobs are then used to develop a novel loss function that instills structure via consensus learning (Section 3.2).

3.1. Face Segmentation Transfer

Transfer data. Unlike [58] that took advantage of an existing yet small labeled set, or [49] that developed tools to assist the manual labeling, we use facial images from the CASIA WebFaces [69], VGG Faces [52] and MS-Celeb-1M [21] to harvest occlusions in-the-wild without any human effort. We argue that manually annotating them pixel-wise is a painstaking effort and practically infeasible. To pre-train our model, we used 539,960 training images and 58,306 validation images without overlapping subjects. In the following sections we explain how we coped with the ambiguous and noisy synthesized pseudo-labels.

Factorizing out occlusions. We express the occlusion appearing in a face image \mathbf{I} as the residual ρ obtained from the difference between the full face contour mask \mathbf{f} and the face segmentation mask \mathbf{f}^{occ} provided by [49]. More formally, given \mathbf{I} we further segment it as:

$$\rho \approx [\mathbf{f} - \mathbf{f}^{occ}]_+, \quad \text{where } [\cdot]_+ = \max(0, \cdot). \quad (1)$$

Eq. (1) serves to factorize the occlusions out from the background. The mask \mathbf{f} is expressed as the convex hull of the full face shape predicted by projecting onto the image a generic face shape via 3D perspective projection [45] computed using the robust method mentioned in [8]. Note that since we are interested in the facial outer contour, [8] fits our needs since it favors robustness to precision—which is especially useful in the presence of occlusions. This is easily implemented by obtaining the predicted pose $\mathbf{K}[\mathbf{R}|\mathbf{t}]$ and projecting 64 vertices onto the image corresponding to the

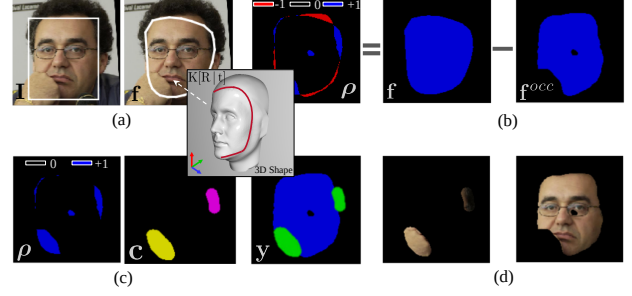


Figure 2: Factorizing out occlusions. (a) We use face detection and a strong prior provided by the projection of a 3D facial shape to obtain the full face mask; (b) The initial ρ residual is expressed as the difference between the full and the segmentation mask; (c) The residual is further refined and its connected components \mathbf{c} estimated; (d) Label mask \mathbf{y} is obtained from \mathbf{c} to decouple the occlusions from the face.

3D contour of the face (jawlines plus forehead). Then, \mathbf{f} is efficiently computed finding the simplex of the convex-hull and probing to find if a matrix index (i, j) of \mathbf{f} is outside the hull. By construction, the residual takes values in $\{-1, 0, +1\}$ and is then truncated to $\{0, 1\}$ as stated in Eq. (1) to remove possibly ambiguous labels. The residual then undergoes a series of morphological operations to amplify the occlusions, since, for example, in face completion applications [37, 35] over-segmentation of occlusions is preferable over under-segmentation. The final ρ is obtained by applying an erode operator twice with rectangular kernels of size 25×7 and a dilation operation with elliptical kernel of size 45×45 . The values are chosen to be conservative with respect to the occlusions: in case the teacher network undersegments occlusions, the rationale was to amplify the occlusions over the face regions. Finally, the connected components $\mathcal{O}(\rho)$ are estimated from the residual to identify main blobs or objects on the face. By merging the output of the face segmentation network \mathbf{f}^{occ} and the labels provided by the connected components $\mathcal{O}(\rho)$, the method yields a pseudo-ground-truth mask $\mathbf{c}(\mathbf{I}) \in \mathbb{R}^{1 \times H \times W}$, where \mathbf{c} takes values in $\{0, \dots, N_c\}$. Note that, N_c is not constant since the number of blobs—i.e., connected components—varies across images; yet by construction, we have that the pixel-wise semantic labels are defined as:

$$\forall i, j \quad \mathbf{y}(i, j) = \begin{cases} (i, j) \sim \text{background}, & \text{if } \mathbf{c}(i, j) = 0, \\ (i, j) \sim \text{face}, & \text{if } \mathbf{c}(i, j) = 1, \\ (i, j) \sim \text{occlusion}, & \text{if } \mathbf{c}(i, j) \geq 2. \end{cases} \quad (2)$$

The entire process is summarized in Fig. 2.

3.2. Enforcing Structure via Consensus Learning

Network structure. We employ a network based on a fully convolutional encoder-decoder [56] taking as input 128×128 RGB images. The network uses recur-

rent applications of a basic building block of Conv–Elu–BatchNorm [13]. The model has two encoding branches: a first encoding branch increases the depth while decreasing spatial dimension up to $256 \times 32 \times 32$. The second sub-encoder refines the feature maps of the first encoder focusing the attention on a wider part of the input face, using two blocks with dilated convolutions [70]. The feature maps of the two encoders are concatenated together. The decoder maps back to the input spatial dimension using efficient sub-pixel convolution [61] with upscaling ratio of two to upscale the feature maps. Importantly, a final pixel in the classification layer has a receptive field in the input image of 121 pixels, hence it almost covers the entire face².

A critique of pixel-wise loss functions. The general recipe for semantic segmentation boils down to transforming an image \mathbf{I} using a network ϕ that generates a $K \times H \times W$ tensor of probabilities to maximize the conditioned probability of the ground-truth mask \mathbf{y} with size $1 \times H \times W$. The network output is expressed as a set of multinoulli³ distributions, where each pixel prediction $(i, j) \sim \text{Cat}(K, p)$. The fitting to the mask labels is implemented with softmax plus cross-entropy, applied pixel-wise and finally averaged over the final tensor. This introduces a strong assumption: all the final generated pixels in the mask behave as independent and identically distributed (i.i.d.) random variables, which violates the regular structures implicitly present in nature [16, 25]. The expected loss across all pixel’s image $\mathbb{E}[\ell(\cdot)]$ is eventually:

$$\begin{aligned} \frac{1}{HW} \sum_{i=1}^H \sum_{j=1}^W \ell(i, j) &= \frac{1}{HW} \sum_{i=1}^H \sum_{j=1}^W \mathcal{H}(\mathbf{p}_{i,j}, \mathbf{y}_{i,j}) = \\ &= -\frac{1}{HW} \sum_{i=1}^H \sum_{j=1}^W \mathbf{y}_{i,j} \log(\mathbf{p}_{i,j}), \quad (3) \end{aligned}$$

where \mathcal{H} indicates the cross-entropy between the predicted softmax probability $\mathbf{p}_{i,j}$ at a pixel (i, j) and \mathbf{y} is one-hot encoding of the class membership. More analytically:

$$\mathbb{E}[\ell(\cdot)] = -\frac{1}{HW} \sum_{s \in \mathbf{y}} \log \left(\frac{e^{\mathbf{W}_{(k^*, s)} \mathbf{x}_{(k^*, s)}^T}}{\sum_{k=1}^K e^{\mathbf{W}_{(k, s)} \mathbf{x}_{(k, s)}^T}} \right), \quad (4)$$

where k runs over the classes, k^* selects the ground-truth class index, and s runs on all the pixels. \mathbf{W} represents the final classification convolutional layer mapping to the label space and \mathbf{x} the activation before \mathbf{W} .

Eq. (4) assumes that the prediction at a given pixel is not regularized by the structure present in the input, and

²For additional details on the network architecture please check the supplementary material in Appendix A.

³Generalization of Bernoulli distribution with K categories, also known as categorical distribution.

hence it suggests improvement by incorporating smoothness constraints. Although each pixel prediction in \mathbf{x} has some knowledge of the neighbour pixels in the input image, given the recurrent application of convolutions, this is not enough to avoid predicting pixels independently, even in the dilated case [70, 71] allowing for large receptive fields as in our model. Despite the recent progress in semantic segmentation [12], the aforementioned issue is not yet fully addressed in the face domain. Eq. (4) is also often used in applications such as face segmentation, face parsing or occlusion detection, and in many cases where the network has to densely label pixels. The problem of returning sparse predictions is especially important on faces, since this exhibits a very regular structure. The same is true for occlusion covering the face: obstructing objects covering the face are rarely composed of sparse tiny parts, yet rather show up with continuous shapes.

Preliminaries. The above problem calls for a solution regarding the independent assumption of the predictions in Eq. (4), even more in the face domain. Unlike [58, 49] that couple the background and occlusion classes together, we define face segmentation as a three-class problem ($K = 3$) aiming to classify background \mathbf{B} , face \mathbf{F} and occlusion \mathbf{O} . Additionally, following Section 3.1, we allow for occlusions to be modeled as a variable set of blobs over the face $\mathcal{O} = \{\mathbf{O}\}_{i=1}^{N_c}$, where N_c varies given the input \mathbf{I} . In spite of this, Eq. (3) can be rewritten as:

$$\frac{1}{|\mathbf{F}|} \sum_{s \in \mathbf{F}} \ell(s) + \frac{1}{|\mathbf{B}|} \sum_{s \in \mathbf{B}} \ell(s) + \frac{1}{|\mathcal{O}|} \sum_{\mathbf{O} \in \mathcal{O}} \left(\frac{1}{|\mathbf{O}|} \sum_{s \in \mathbf{O}} \ell(s) \right), \quad (5)$$

where $\ell(s)$ corresponds to the softmax plus cross-entropy loss at a pixel s , that runs over all the pixels in each blob, and $|\cdot|$ counts the pixels of a blob. Eq. (5) is identical to Eq. (3), with the only difference being that the spatial frequency of each component is marginalized out, or in other terms, having the same weights for all blobs irrespective of their size. Next, we explain how to enforce smoothness in our training process.

Enforcing structure in each blob. The core idea behind our method is shown in Fig. 3. We define the expected probability $\mathbb{E}[p]$ on a blob \mathbf{O} as:

$$\hat{p}_{\mathbf{O}} \doteq \frac{1}{|\mathbf{O}|} \sum_{s \in \mathbf{O}} p(s) = \frac{1}{|\mathbf{O}|} \sum_{s \in \mathbf{O}} \left(\frac{e^{\mathbf{W}_{(k^*, s)} \mathbf{x}_{(k^*, s)}^T}}{\sum_{k=1}^K e^{\mathbf{W}_{(k, s)} \mathbf{x}_{(k, s)}^T}} \right), \quad (6)$$

that corresponds to the average conditioned probability over all the pixels of the blob \mathbf{O} . Note that the values in Eq. (6) remain positive and the mass of $\hat{p}_{\mathbf{O}}$ sums up to one. Then, we can augment Eq. (3) in the following way: given a blob

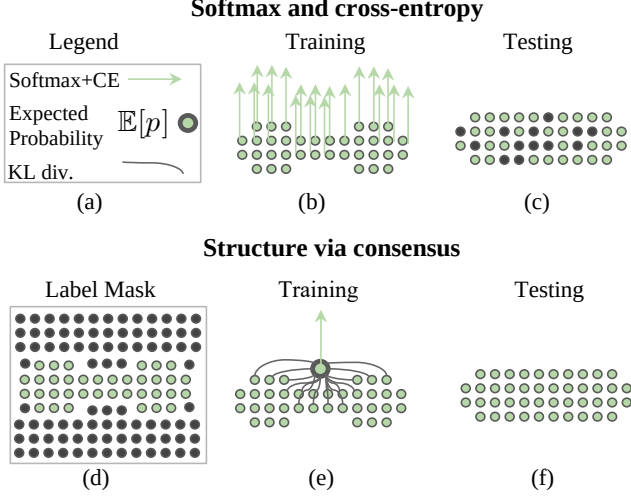


Figure 3: Intuition behind our loss. (a) legend; (b) regular training proceeds pixel-wise, *independently* and enforces densely each pixel to fit the label (no notion of smoothness of the object); (c) this leads to sparse prediction at test time for unseen objects; (d) pixel-wise labels for an image; (e) we force the expected prediction in a blob $\mathbb{E}[p]$ to the label, yet ensure no deviation of each pixel from the average; (f) the network is better regularized for segmenting *with less sparse predictions*.

on the mask we can define the loss on the blob as:

$$\underbrace{\alpha \cdot D_{KL}(\mathbf{y} \parallel \hat{\mathbf{p}}_{\mathbf{O}})}_{\text{1st order; matches the class label}} + \underbrace{\beta \cdot \frac{1}{|\mathbf{O}|} \sum_{s \in \mathbf{O}} D_{KL}(\hat{\mathbf{p}}_{\mathbf{O}} \parallel p_s)}_{\text{2nd order; ensures no deviation}}, \quad (7)$$

where α, β are two hyper-parameters controlling the trade-off between matching the labels and ensuring consensus and D_{KL} denotes the Kullback-Leibler divergence. Putting this all together, indicating all the blobs (background \mathbf{B} , face \mathbf{F} , occlusions \mathbf{O}) as \mathbf{c} , our method finally optimizes:

$$\frac{1}{|\mathbf{C}|} \sum_{\mathbf{O} \in \mathbf{c}} \left[\alpha D_{KL}(\mathbf{y} \parallel \hat{\mathbf{p}}_{\mathbf{O}}) + \frac{\beta}{|\mathbf{O}|} \sum_{s \in \mathbf{O}} D_{KL}(\hat{\mathbf{p}}_{\mathbf{O}} \parallel p_s) \right]. \quad (8)$$

Note that although here we apply our formulation specifically to face segmentation/occlusion detection, if the method is provided with a set of blobs, then it can be applied more broadly. Section 4 shows how to easily obtain blobs from the available labels in standard benchmarks for a full generalization to the face parsing problems.

3.3. Interpretations

Eq. (7) can be interpreted as follows: given a blob on the mask \mathbf{O} , we enforce that the average of the predictions over the blob has to match the class label $D_{KL}(\mathbf{y} \parallel \hat{\mathbf{p}}_{\mathbf{O}})$ —as a sort of first-order momentum—plus a second term ensures

that all pixel-wise probabilities inside the blob are close to its average, i.e., $\sum_{s \in \mathbf{O}} D_{KL}(\hat{\mathbf{p}}_{\mathbf{O}} \parallel p_s)$. We treat each blob as a whole using the first term and we enforce smoothness using the regularization of the second term: unlike the baseline, our loss connects all the pixel predictions in a blob with the average prediction, defining implicit inter-dependencies between predictions as a sort of regularizer.

Implementation. In the first term, what is actually implemented as D_{KL} is the negative log-likelihood of the ground-truth probability from $\hat{\mathbf{p}}_{\mathbf{O}}$. This can still be viewed as KL div since this latter reduces to cross-entropy given that they are related as $D_{KL}(\mathbf{y} \parallel \hat{\mathbf{p}}_{\mathbf{O}}) \doteq \mathcal{H}(\mathbf{y}, \hat{\mathbf{p}}_{\mathbf{O}}) - \mathcal{H}(\mathbf{y})$, and, \mathbf{y} , the target distribution, is a one-hot encoding, thus with entropy equal to zero. Hence, KL div. is equal to cross-entropy in this particular case and implement using negative log-likelihood of the ground-truth index class on $\hat{\mathbf{p}}_{\mathbf{O}}$. The second term in Eq. (7) is simply implemented as KL div. between two discrete distributions. In this sense, Eq. (7) keeps an elegant consistency across its two terms, without requiring the system for external CRF post-processing or additional parameters to perform adversarial training.

Interpretation as a generalization of Eq. (4). Additionally, the proposed formulation can be seen as a generalization of Eq. (4). A pixel-wise loss coincides with a boundary case of our loss when all the blobs collapse down to each pixel. In this case, each pixel matches the class label—first term in Eq. (7)—and the second term collapses to zero, since, by definition, a pixel is consistent to itself.

Connection to CRFs. Our formulation shares some similarities with seminal CRFs [6, 63, 41] and graph cut [4, 5] for semantic segmentation. At first sight the two terms in Eq. (7) are reminiscent of minimizing the energy of a function ϕ as $E_{data}(\phi) + E_{smooth}(\phi)$, as proposed in [5]. Though the CRF has already been used in conjunction with a ConvNet (e.g., [74, 11]), we do share the core philosophy with novel traits; unlike [5], our “unary potential” is not defined on single pixels but on the expected probability over the shape, and our “pair-wise potential” is not defined on pairs of *adjacent pixels* [5] or *fully connected* [11], yet is constrained by components with characteristic shapes. We note here that in our case ϕ is parameterized by the filters of a ConvNet. Finally, we acknowledge that CRFs captures long range interactions via a fully-connected graphical structure, in contrast, the proposed loss only captures constraints within neighborhoods; though, the “neighborhood” in our case can be small or large depending on the label masks or connected components mined in Section 3.1. In light of this, our formulation still exhibits innovative traits with respect to seminal work.

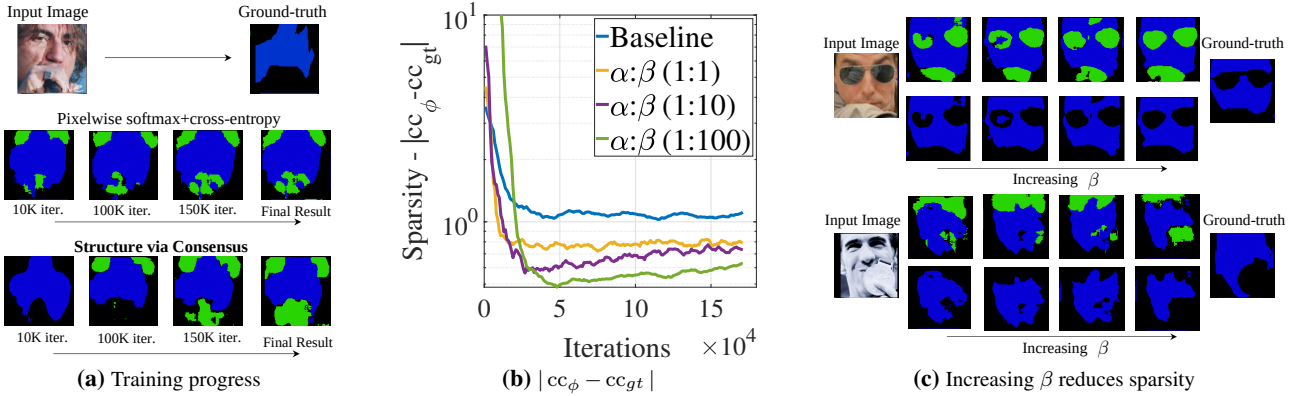


Figure 4: More regular, smooth structure learned; (a) As the training progresses, our method learns more regular, smooth structure which yields a more regular mask when compared to the pixel-wise baseline (sample from the COFW test set); (b) less sparsity is confirmed by visualization of the error in the number of connected components between the predicted cc_ϕ and annotated mask cc_{gt} . A higher weight on β greatly decreases the sparsity of the masks (c) this effect is confirmed when inspecting qualitative samples from the COFW test set.

4. Experimental Evaluation

We report results of ablation studies or other experiments that motivated our choices, along with state-of-the-art evaluations on publicly available and commonly used benchmarks for face segmentation, occlusion detection and face parsing. Our approach surpasses previous state-of-the-art by wide margins on the COFW (Caltech Occluded Faces in the Wild) [7] and shows comparable results on the Part Labels set [29].

4.1. Implementation Details

Face preprocessing. We used a minimalist face preprocessing, thereby simply applying a face detector [68] and using the adjusted square box to crop the face to roughly compensate for scale and translation for a final 128×128 image.

Training. To pre-train the network we use the Adam optimizer [32], starting from a learning rate of $1e-3$ and finishing with $1e-5$. Pseudo-labels are provided following Section 3.1. A scheduler checks the pixel-wise average recall across classes on the validation and decreases the learning by $1e-1$ when the above metric plateaus. All the models are trained with a batch size of 128.

When fine-tuning on COFW, we apply our face segmentation transfer (Section 3.1) to identify the main blobs without applying the morphological operations to use the fine-grain human annotated masks. In other tests, we simply treat the separate mask classes as the blobs. On COFW we used a flat learning rate of $1e-5$, while on PartLabel $1e-4$. All the models train until convergence reaches saturation. Remarkably, important parameters in Eq. (7) are α , β that are set as $\{10:5\}$ in all our experiments, as we found these values to be a good trade-off between enforcing smoothness and fitting the labels to guarantee high accuracy.

4.2. Supporting Experiment

More regular, less scattered structure. Fig. 4a shows qualitatively the difference in the prediction between the baseline and learning with *structure via consensus* on a COFW [7] test sample when performing transfer learning with our loss. The sample is chosen for its difficulty in the face segmentation task (the occlusion appears fragmented—although it is not—and is of similar color to the face, in spite of the fact that it is made by two continuous objects (e.g., hands and microphone). As the training progresses, our method offers more continuous segmentation masks that, in turn, become a better face segmentation, without sparse holes. Our claim is supported by Fig. 4b, showing the average absolute error $\frac{1}{N} \sum_i^N |cc_\phi - cc_{gt}|$ between the number of connected components in the ground-truth mask (cc_{gt}) and the components dynamically computed on our prediction (cc_ϕ) at every iteration. The error is averaged across all the testing samples and provides a valuable understanding of the sparsity of the prediction and confirms that increasing our smooth term β in Eq. (8) induces a significant less sparse output. Fig. 4b shows the trend of the sparsity error measure as the training evolves for different β values. Additional qualitative samples in Fig. 4c further support our hypothesis.

4.3. Caltech Occluded Faces in the Wild

Comparison with the state-of-the-art. We use the COFW set [7] for proving the effectiveness of our method. COFW consists of 500 labeled images for training and 507 for testing. Labels consist of binary, pixel-level face segmentation masks. Table 1 reports our results compared to the state-of-the-art, along with ablation studies we conducted to motivate our choices. The table reports figures for face IOU intersection over union (or Jaccard index), pixel accuracy

Method	IOU _{face}	acc.	rec _{face}	rec _{all}	spars.	fps
Struct. Forest [28]	—	83.9	—	88.6	—	—
RPP [67]	72.4	—	—	—	—	0.03
SAPM [17]	83.5	88.6	87.1	—	—	—
Liu <i>et al.</i> [41]	72.9	79.8	89.9	77.9	—	0.29
Saito <i>et al.</i> [58] +GraphCut	83.9	88.7	92.7	—	—	43.2
Nirkin <i>et al.</i> [49]	81.6	87.4	93.3	—	—	48.6
Nirkin <i>et al.</i> [49] +Occ. Aug.	83.7	88.8	94.1	87.4	—	48.6
Softmax+CE +Scratch	76.8	83.7	86.9	82.6	3.5	300
Softmax+CE +Transf.	84.5	89.4	93.3	88.1	1.0	300
Softmax+CE +Transf.+f.t.	84.1	89.4	90.3	89.1	3.8	300
Struct. via con. +Transf.+f.t.	85.7	90.4	92.5	89.7	1.6	300
Struct. via con. +Transf.+f.t.+reg.	87.0	91.3	92.4	90.9	0.8	300

Table 1: COFW set. Occlusion segmentation results.

(acc.), pixel-wise recall of the face class (rec_{face}),⁴ average pixel-wise recall across *all classes* (rec_{all}) face and non-face, our measure of sparsity ($\frac{1}{N} \sum_i^N |cc_\phi - cc_{gt}|$) and fps (frames per second). When we test our method we simply merge the responses from the occlusion class and background class as a single non-face class. Following previous work [28, 67, 17], we report the metric in the face box provided with COFW.

Given the small size of COFW, it is challenging for a deep model to adjust its weights given only hundreds of samples. To prove this point, and, more importantly, to motivate Section 3.1, we ran a simple experiment by training from random weights (+Scratch). Since we are updating the weights very slowly, the model is able to learn, yet reaches a result that is too distant from the state-of-the-art. For this reason, previous methods [58, 49] employed other labeled sets [29] or built semiautomatic annotation tools [49] to attain some sort of transfer learning. Similar to them, we perform transfer learning, yet unlike them, we transfer knowledge from [49] as explained in Section 3.1. Results in Table 1 (+Transf.) support our face segmentation transfer. Our method is able to outperform the teacher network [49]. Additionally, if we combine all our novelties and further fine-tune on the 500 samples provided, we obtain an additional positive gap with respect to the state-of-the-art (Struct. via con. +Transf.+F.t.+reg.). Our method reduces the overall error-rate by 27.7% for the metric rec_{all}. As a final note, since we are using a lightweight encoder-decoder, unlike [58], our smoothness constraint is enforced at *training time only*. Our inference time is remarkable compared to recent methods: on average a forward pass takes 3.1 ms yielding more than 300 predicted masks per second (fps).

Ablation study. The effect of learning with “structure via consensus” is shown in Table 1 and is compared to the softmax+CE that most of the methods discussed above rely on.

⁴Starting from [17], only the rec_{face} has been reported on COFW omitting rec_{all}; since a *single* recall class can be made arbitrarily high by just optimizing the system for that class, we strove to report both for fairness.

While fine-tuning with the pixel-wise loss increases sparsity (1.0 \rightarrow 3.8) on the masks and actually *reduces performance*; on the contrary, by enforcing smoothness with our loss, we are able to better generalize to the test set, to improve over the transfer learning and to keep a lower sparsity (1.6). Further gain is obtained by regularizing the model with dropout and flip augmentation (+reg.). A qualitative comparison on COFW is shown in Fig. 5, where our method shows more structured masks than the baseline and [49]. Other qualitative samples are shown in Figs. 1, 4a and 4c.

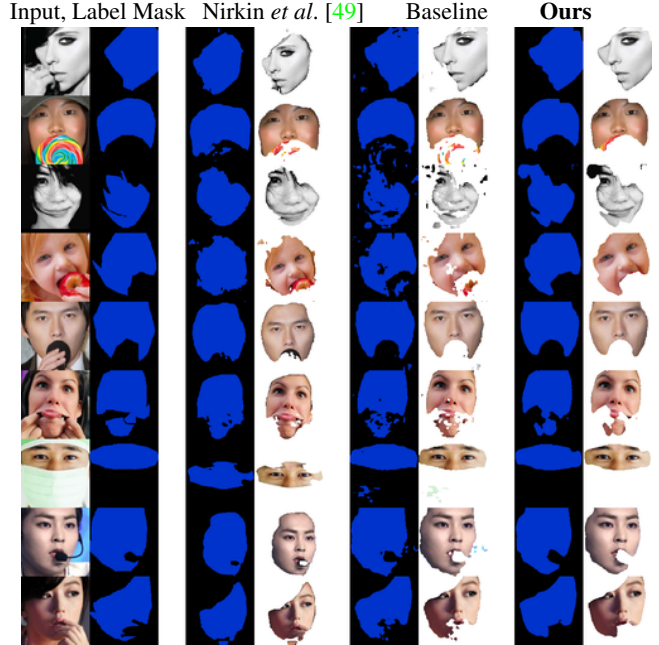


Figure 5: Qualitative samples from the COFW set. Input image and its ground-truth mask; results by Nirkin *et al.* [49]; baseline with pixel-wise loss; our result. The faces are masked to remove occlusions according to each method. Additional results in the supplementary material in Appendix B.

4.4. Part Labels Database

Comparison with the state-of-the-art. Labeled Faces in the Wild (LFW) [23] is a well-known face set comprising more than 13,000 images of faces in the wild initially developed for face recognition. Following previous work [29], we employ the funneled version of the set, in which images have already been coarsely aligned. The database is a subset of the challenging LFW for face segmentation, is proposed in [29], and consists of 1,500 training, 500 validation, and 927 testing images. The images are labeled with efficient super-pixel segmentation though the labels are quite accurate. The set provides three classes—background, hair/facial-hair and face/neck along with the corresponding super-pixel mapping. We fine-tune our system on the 2,000 train/val images and test on the 927 evaluation faces

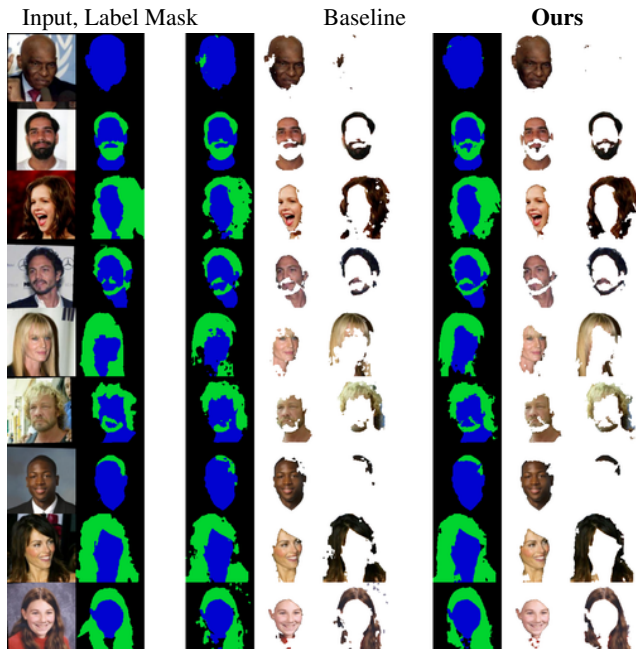


Figure 6: Qualitative results from the Part Labels set. Input image and its ground-truth mask; results by the baseline with pixel-wise loss; our result. The faces are masked to decouple the face from the hair. Additional results in the supplementary material in Appendix C.

following the publicly available splits. To have a thorough comparison with current work, we report both pixel-wise (acc_p) and super-pixel-wise accuracies (acc_{sp}). To report the super-pixel accuracy, we select the most frequent predicted label in a super-pixel. Our system reports results on par or above the state-of-the-art with the important notation that in our case we perform *direct inference* (no CRF \checkmark), and we are *not forcing any smoothness* via CRF at test-time. Table 2 shows the state-of-the-art evaluation. We obtain pixel accuracy above the current practice and super-pixel accuracy on-par. We have results similar to Tsogkas *et al.* [64], yet they use a CRF to smooth out the result. Notably, our approach shows similar or above numbers when compared with the active research of adversarial training (following the extensive experimentation from [51]), though this latter requires more parameters to train because of the discriminator.

Ablation Study. All the aforementioned metrics are almost saturated, so it is instructive to show where our method really shines. In Table 3 we additionally report ablation study showing the impact of our loss: in general pixel accuracy increases with our loss but since these metrics do not take into account class frequencies, we also recorded the IOU per class. Using “structure via consensus” the IOU for hair class goes up from 68.95% to 72.48%. The same is reflected in the mean IOU over classes—from 83.65% to 85.74%.

Method	size _{in}	No CRF	acc _p	acc _{sp}
Gygli <i>et al.</i> [22] — DVN	32	\checkmark	—	92.44
Gygli <i>et al.</i> [22] — FCN baseline	32	\checkmark	—	95.36
Kae <i>et al.</i> [29] — CRF	250	\times	—	93.23
Kae <i>et al.</i> [29] — Glog	250	\times	—	94.95
Liu <i>et al.</i> [41]	250	\times	95.24	—
Liu <i>et al.</i> [40] — RNN	128	\checkmark	95.46	—
Liu <i>et al.</i> [40, 10] — CNN-CRF	128	\times	92.59	—
Saxena <i>et al.</i> (sparse) [60]	250	\checkmark	94.60	95.58
Saxena <i>et al.</i> (dense) [60]	250	\checkmark	94.82	95.63
Zheng <i>et al.</i> [73] — CNN-VAE	250	\checkmark	—	96.59
Tsogkas <i>et al.</i> [64] — CNN	250	\checkmark	—	96.54
Tsogkas <i>et al.</i> [64] — RBM+CRF	250	\times	—	96.97
Adversarial Training				
FCN — GAN [19]	250	\checkmark	—	95.53
GAN [19]	250	\checkmark	—	95.54
FCN — LSGAN [44]	250	\checkmark	—	95.51
LSGAN [44]	250	\checkmark	—	95.52
FCN — WGAN,GP [20]	250	\checkmark	—	95.59
WGAN,GP [20]	250	\checkmark	—	95.59
FCN — EBGAN [72]	250	\checkmark	—	95.50
EBGAN [72]	250	\checkmark	—	95.52
FCN — LDRSP [51]	250	\checkmark	—	95.87
LDRSP [51]	250	\checkmark	—	96.47
Structure via Consensus (Ours)	128	\checkmark	96.01	96.73

Table 2: Part Labels set. The comparison of pixel and super-pixel accuracies (acc_p , acc_{sp}) between ours, state-of-the-art and adversarial learning methods on the Label Part database. The input size and usage of smoothness via CRF are emphasized.

Method	IOU _{hair}	IOU _{bg}	IOU _{face}	IOU _{mean}	recall _{all}	acc _p	acc _{sp}	spars.
Softmax+CE	68.95	94.41	87.60	83.65	90.41	94.77	96.15	15.86
Struct. via cons.	72.48	95.17	89.98	85.74	91.26	95.55	96.61	13.66
Softmax+CE +reg.	73.97	95.52	89.81	86.46	92.50	95.77	96.62	3.3
Struct. via cons. +reg.	75.76	95.69	90.50	87.32	93.38	96.01	96.73	3.3

Table 3: Ablation study on Part Labels set. Detailed ablation study on the Part Label set for the base model and a model with additional regularization (+reg.).

We repeated the same experiments further regularizing the model with dropout and flip augmentation (+reg.), our loss provided a similar improvement, and, importantly, the boost is consistent in all the metrics. Notably in all these ablations, our method provided less sparse masks when compared to the baseline as reported in Table 3 under the sparsity metric, exhibiting less over-fitting than the baseline.

Qualitative results on the Part Labels set are shown in Fig. 6 and compared to the baseline: our hair segmentation exhibits less fragmented segments and fewer holes than the baseline, yet yielding an excellent face segmentation.

5. Conclusions and Future Work

We have proposed a novel method that aids face segmentation, building on the novel concept of learning structure via consensus. Our approach exhibits figures on par or above the state-of-the-art. Our future work is to experiment

with Pascal VOC [14] on the generic task of semantic segmentation, thereby using the available instance-level segmentation of objects to port our loss to work with generic objects. Currently the system is using blobs as a constraint for the consensus, and those are given as input to the system through an automatic, noisy preprocessing step or by some form of human supervision from the annotations. As a more long-term future work, we envision the possibility of learning to cluster pixels of same objects in an unsupervised fashion without the need for instance-level annotations.

Acknowledgements. This research is based upon work supported by the Office of the Director of National Intelligence (ODNI), Intelligence Advanced Research Projects Activity (IARPA), via IARPA R&D Contract No. 2017-17020200005. The views and conclusions contained herein are those of the authors and should not be interpreted as necessarily representing the official policies or endorsements, either expressed or implied, of the ODNI, IARPA, or the U.S. Government. The U.S. Government is authorized to reproduce and distribute reprints for Governmental purposes notwithstanding any copyright annotation thereon. The authors would like to thank Shay Deutsch, Ayush Jaiswal, Hengameh Mirzaalian, Mohamed Hussein, Leonidas Spinoulas and the anonymous reviewers for their helpful discussions.

A. Network Architecture

Architecture Details. Further details of our network architecture are provided in Table 4. Our network is similar to the encoder-decoder framework U-Net [56], but it has some modifications explained below. The input resolution is 128×128, though our model can work also at 256×256 since it is fully convolutional. The resolution is decreased only with striding without any pooling layer. The basic block of the network consists of ReflectionPad2, Convolution, ELU [13] and Batch Normalization. The first encoder downsamples the input up to 32×32 to preserve some spatial information, with a depth of 256 (layer id 19 referring to Table 4); then other convolutional layers with dilation set to 4 and 3 in a sub-encoder refine the feature maps to capture a more global scale (layer id 27 referring to Table 4). In Table 4, if not specified, convolution is computed with dilation equal to 1. The final feature maps are concatenated together for a final bottleneck feature map with dimensionality 512×32×32. The convolutional filters are initialized with the method described in [18]. The decoder part takes the bottleneck feature maps as input and upscales it back to the input dimension. We used efficient sub-pixel convolution with ratio equal to 2 applied two times in the decoder to do this upscaling, since sub-pixel convolution has been shown to work well in super-resolution applications. We

ID	Layer (type)	Output Shape ($B \times C \times H \times W$)	Param. Size
Encoder ↓			
1	ReflectionPad2d	[64, 3, 130, 130]	—
2	Conv2d	[64, 64, 128, 128]	1,792
3	ELU	[64, 64, 128, 128]	—
4	ReflectionPad2d	[64, 64, 130, 130]	—
5	Conv2d	[64, 128, 64, 64]	73,856
6	ELU	[64, 128, 64, 64]	—
7	BatchNorm2d	[64, 128, 64, 64]	256
8	ReflectionPad2d	[64, 128, 66, 66]	—
9	Conv2d	[64, 128, 64, 64]	147,584
10	ELU	[64, 128, 64, 64]	—
11	BatchNorm2d-	[64, 128, 64, 64]	256
12	ReflectionPad2d-	[64, 128, 66, 66]	—
13	Conv2d	[64, 128, 64, 64]	147,584
14	ELU	[64, 128, 64, 64]	—
15	BatchNorm2d-	[64, 128, 64, 64]	256
16	ReflectionPad2d	[64, 128, 66, 66]	—
17	Conv2d	[64, 256, 32, 32]	295,168
18	ELU	[64, 256, 32, 32]	—
19	BatchNorm2d	[64, 256, 32, 32]	512
Sub-encoder ↓			
20	ReflectionPad2d	[64, 256, 40, 40]	—
21	Conv2d (dilation=4)	[64, 256, 32, 32]	590,080
22	ELU	[64, 256, 32, 32]	—
23	BatchNorm2d	[64, 256, 32, 32]	512
24	ReflectionPad2d	[64, 256, 38, 38]	—
25	Conv2d (dilation=3)	[64, 256, 32, 32]	590,080
26	ELU	[64, 256, 32, 32]	—
27	BatchNorm2d	[64, 256, 32, 32]	512
Concat feature maps 19 and 27			
Decoder ↑			
28	ReflectionPad2d	[64, 512, 34, 34]	—
29	Conv2d	[64, 512, 32, 32]	2,359,808
30	ELU	[64, 512, 32, 32]	—
31	BatchNorm2d	[64, 512, 32, 32]	1,024
32	<i>PixelShuffle</i> (×2)	[64, 128, 64, 64]	—
33	ReflectionPad2d	[64, 128, 66, 66]	—
34	Conv2d	[64, 128, 64, 64]	147,584
35	ELU	[64, 128, 64, 64]	—
36	BatchNorm2d	[64, 128, 64, 64]	256
37	ReflectionPad2d	[64, 128, 66, 66]	—
38	Conv2d	[64, 128, 64, 64]	147,584
39	ELU	[64, 128, 64, 64]	—
40	BatchNorm2d	[64, 128, 64, 64]	256
41	<i>PixelShuffle</i> (×2)	[64, 32, 128, 128]	—
42	ReflectionPad2d	[64, 32, 130, 130]	—
43	Conv2d	[64, 32, 128, 128]	9,248
44	ELU	[64, 32, 128, 128]	—
45	ReflectionPad2d	[64, 32, 130, 130]	—
46	Conv2d	[64, 32, 128, 128]	9,248
47	ELU	[64, 32, 128, 128]	—
48	Conv2d	[64, 3, 128, 128]	867
Total # params.			4,524,323

Table 4: Network details. Network layers, output shapes and learnable parameters.

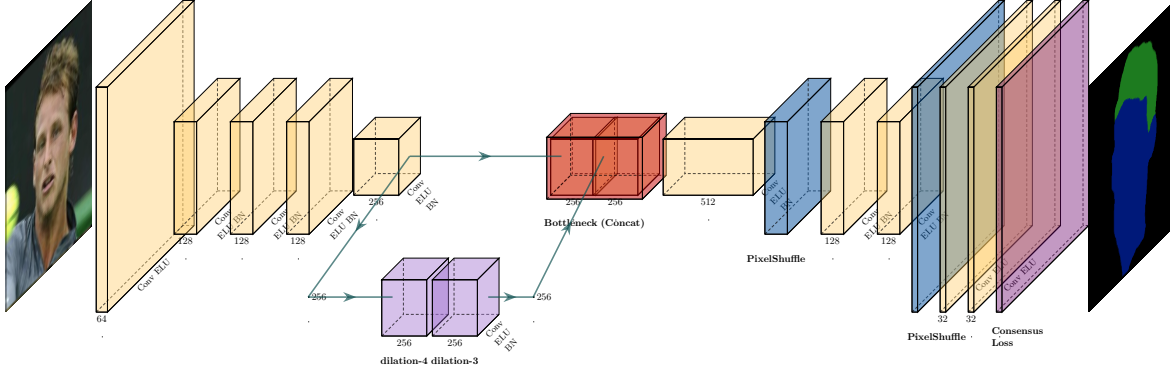


Figure 7: Network structure at a glance. Encoder-decoder used for face segmentation and supervised through structure via consensus.

used Pytorch [53] to develop the network and sub-pixel convolution has been implemented via `PixelShuffling`.⁵ The entire encoder-decoder has 4,524,323 parameters. The network is supervised either with 2D softmax normalization and cross-entropy or by using our novel “structure via consensus” method. The final network structure is displayed at a glance in Fig. 7 using [26].

B. Additional Qualitative Results on COFW

We show supplementary results on the Caltech Occluded Face in the Wild data (COFW) [7] in Fig. 8. The figures augment Fig. 5 in the paper to provide further samples. The figures display the input image and its ground-truth mask; the result obtained by Nirkin *et al.* [49], obtained by aligning the faces as the mentioned in their publicly available code; our baseline with pixel-wise softmax and cross-entropy; our final approach trained with structure via consensus. Fig. 8 show again that even on a larger pool of samples, our method returns less sparse, more continuous occlusion masks for better face segmentation and parsing. As a remark, we get such clean masks, much closer visually to the ground-truth compared to other approaches, yet we do so by *still* performing pixel-wise inference: we do not use any super-pixel approach at test time nor employ any post-processing step such as CRF, morphological operations etc.

C. Additional Qualitative Results on Part Labels

We show some supplementary qualitative results on the Part Labels database [29] in Fig. 9. On average our masks look more continuous and greatly improve the IoU of the hair class. Fig. 9 reports the input image, the ground-truth annotated mask, the baseline model trained with pixel-wise loss and regularization and our method with regularization. The result of each prediction for each class is used for seg-

menting part of the face showing the segmentation separately for face and hair. In some cases, the predictions of our model are better than the super-pixel labels (e.g. tenth row).

⁵pytorch.org/docs/stable/nn.html#torch.nn.PixelShuffle



Figure 8: Additional qualitative samples from the COFW. Input image and its ground-truth mask; results by Nirkin *et al.* [49]; baseline with pixel-wise loss; our result. The faces are masked to remove occlusions according to each method.

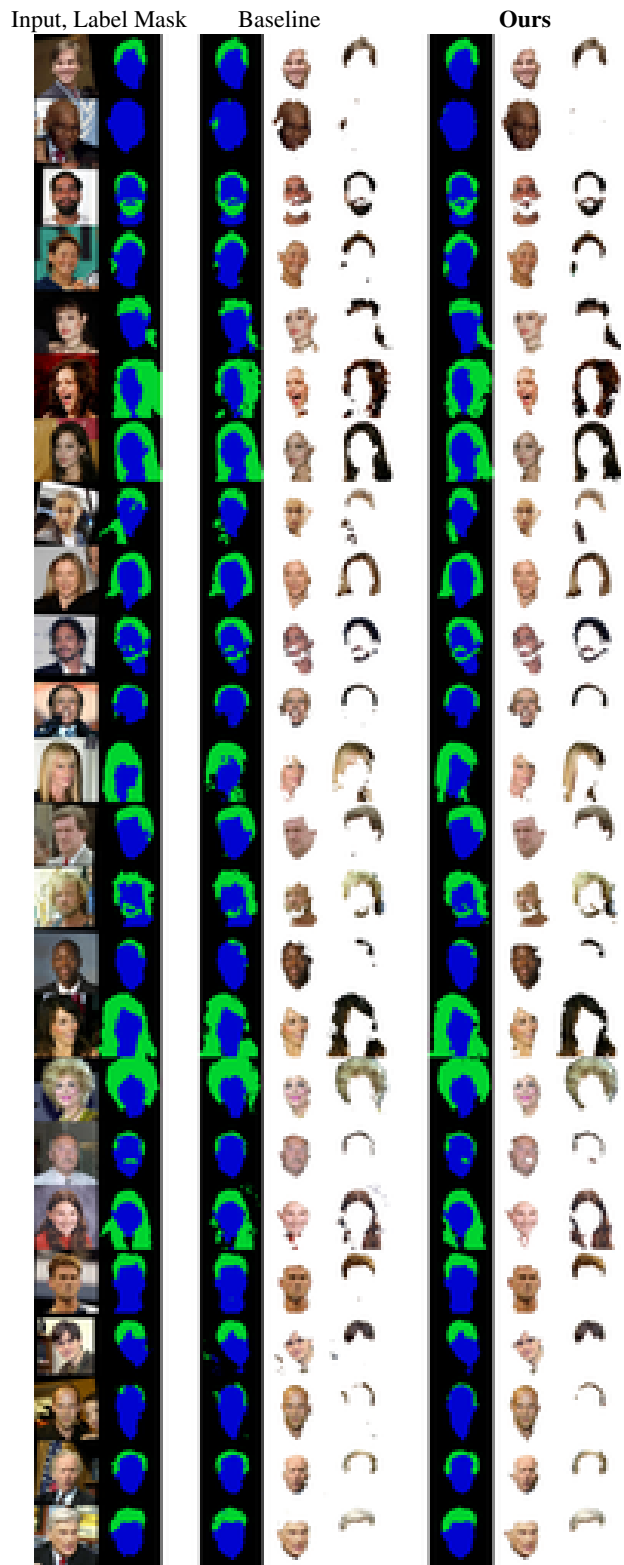


Figure 9: Additional qualitative samples from PartLabel. Input image and its ground-truth mask; results by the baseline with pixel-wise loss; our result. The faces are masked to decouple the face from the hair.

References

- [1] G. Bertasius, J. Shi, and L. Torresani. Semantic segmentation with boundary neural fields. In *CVPR*, 2016. 2
- [2] G. Bertasius, L. Torresani, S. X. Yu, and J. Shi. Convolutional random walk networks for semantic image segmentation. In *CVPR*, 2017. 2
- [3] T. Binford and J. Tenenbaum. Visual perception by computer. In *IEEE Conference on Systems and Control*, 1971. 2
- [4] Y. Boykov, O. Veksler, and R. Zabih. Fast approximate energy minimization via graph cuts. In *ICCV*, volume 1, pages 377–384, 1999. 2, 5
- [5] Y. Boykov, O. Veksler, and R. Zabih. Fast approximate energy minimization via graph cuts. *TPAMI*, 23(11):1, 2001. 2, 5
- [6] Y. Y. Boykov and M.-P. Jolly. Interactive graph cuts for optimal boundary & region segmentation of objects in nd images. In *ICCV*, 2001. 2, 5
- [7] X. P. Burgos-Artizzu, P. Perona, and P. Dollár. Robust face landmark estimation under occlusion. In *ICCV*, pages 1513–1520. IEEE, 2013. 2, 6, 10
- [8] F. Chang, A. Tran, T. Hassner, I. Masi, R. Nevatia, and G. Medioni. FacePoseNet: Making a case for landmark-free face alignment. In *ICCV Workshops*, 2017. 2, 3
- [9] L.-C. Chen, J. T. Barron, G. Papandreou, K. Murphy, and A. L. Yuille. Semantic image segmentation with task-specific edge detection using cnns and a discriminatively trained domain transform. In *CVPR*, 2016. 2
- [10] L.-C. Chen, G. Papandreou, I. Kokkinos, K. Murphy, and A. L. Yuille. Semantic image segmentation with deep convolutional nets and fully connected crfs. In *ICLR*, 2015. 8
- [11] L.-C. Chen, G. Papandreou, I. Kokkinos, K. Murphy, and A. L. Yuille. Deeplab: Semantic image segmentation with deep convolutional nets, atrous convolution, and fully connected crfs. *TPAMI*, 40(4):834–848, 2018. 1, 2, 5
- [12] L.-C. Chen, Y. Zhu, G. Papandreou, F. Schroff, and H. Adam. Encoder-decoder with atrous separable convolution for semantic image segmentation. In *ECCV*, September 2018. 1, 2, 4
- [13] D.-A. Clevert, T. Unterthiner, and S. Hochreiter. Fast and accurate deep network learning by exponential linear units (ELUs). In *ICLR*, 2016. 4, 9
- [14] M. Everingham, L. Van Gool, C. K. Williams, J. Winn, and A. Zisserman. The pascal visual object classes (voc) challenge. *IJCV*, 88(2):303–338, 2010. 9
- [15] B. Fulkerson, A. Vedaldi, and S. Soatto. Class segmentation and object localization with superpixel neighborhoods. In *ICCV*, 2009. 2
- [16] G. Galilei. The assayer. *Discoveries and opinions of Galileo*, (s 229):280, 1957. 1, 4
- [17] G. Ghiasi, C. C. Fowlkes, and C. Irvine. Using segmentation to predict the absence of occluded parts. In *BMVC*, pages 22–1, 2015. 7
- [18] X. Glorot and Y. Bengio. Understanding the difficulty of training deep feedforward neural networks. In *International Conference on Artificial Intelligence and Statistics (AISTATS)*, pages 249–256, 2010. 9
- [19] I. Goodfellow, J. Pouget-Abadie, M. Mirza, B. Xu, D. Warde-Farley, S. Ozair, A. Courville, and Y. Bengio. Generative adversarial nets. In *NIPS*, 2014. 2, 8
- [20] I. Gulrajani, F. Ahmed, M. Arjovsky, V. Dumoulin, and A. C. Courville. Improved training of wasserstein gans. In *NIPS*, 2017. 8
- [21] Y. Guo, L. Zhang, Y. Hu, X. He, and J. Gao. Ms-celeb-1m: A dataset and benchmark for large-scale face recognition. In *ECCV*, 2016. 3
- [22] M. Gygli, M. Norouzi, and A. Angelova. Deep value networks learn to evaluate and iteratively refine structured outputs. In *ICML*, 2017. 8
- [23] G. B. Huang, M. Ramesh, T. Berg, and E. Learned-Miller. Labeled faces in the wild: A database for studying face recognition in unconstrained environments. Technical Report 07-49, UMass, Amherst, October 2007. 2, 7
- [24] W.-C. Hung, Y.-H. Tsai, Y.-T. Liou, Y.-Y. Lin, and M.-H. Yang. Adversarial learning for semi-supervised semantic segmentation. In *BMVC*, 2018. 2
- [25] J.-J. Hwang, T.-W. Ke, J. Shi, and S. X. Yu. Adversarial structure matching loss for image segmentation. *arXiv preprint arXiv:1805.07457*, 2018. 2, 4
- [26] H. Iqbal. Harisqbal88/plotneuralnet v1.0.0. Dec 2018. 10
- [27] S. Jégou, M. Drozdal, D. Vazquez, A. Romero, and Y. Bengio. The one hundred layers tiramisu: Fully convolutional densenets for semantic segmentation. In *CVPR Workshops*, pages 11–19, 2017. 1, 2
- [28] X. Jia, H. Yang, K. Chan, and I. Patras. Structured semi-supervised forest for facial landmarks localization with face mask reasoning. In *BMVC*, 2014. 7
- [29] A. Kae, K. Sohn, H. Lee, and E. Learned-Miller. Augmenting CRFs with Boltzmann machine shape priors for image labeling. In *CVPR*, 2013. 1, 2, 6, 7, 8, 10
- [30] T.-W. Ke, J.-J. Hwang, Z. Liu, and S. X. Yu. Adaptive affinity fields for semantic segmentation. In *ECCV*, pages 587–602, 2018. 2
- [31] I. Kemelmacher-Shlizerman. Transfiguring portraits. *ACM Transactions on Graphics (TOG)*, 35(4):94, 2016. 1
- [32] D. Kingma and J. Ba. Adam: A method for stochastic optimization. In *ICLR*, 2014. 6
- [33] W. Kohler. Gestalt psychology. *Psychological research*, (229), 1967. 2
- [34] A. Krizhevsky, I. Sutskever, and G. E. Hinton. Imagenet classification with deep convolutional neural networks. In *NIPS*, 2012. 2
- [35] Y. Li, S. Liu, J. Yang, and M.-H. Yang. Generative face completion. In *CVPR*, 2017. 1, 3
- [36] Y. Li, H. Qi, J. Dai, X. Ji, and Y. Wei. Fully convolutional instance-aware semantic segmentation. In *CVPR*, pages 2359–2367, 2017. 1, 2
- [37] H. Liao, G. Funka-Lea, Y. Zheng, J. Luo, and S. K. Zhou. Face completion with semantic knowledge and collaborative adversarial learning. *arXiv preprint arXiv:1812.03252*, 2018. 1, 3
- [38] G. Lin, A. Milan, C. Shen, and I. Reid. Refinenet: Multi-path refinement networks for high-resolution semantic segmentation. In *CVPR*, pages 1925–1934, 2017. 1, 2

- [39] C. Liu, J. Yuen, and A. Torralba. Nonparametric scene parsing via label transfer. *TPAMI*, 33(12):2368–2382, 2011. 1
- [40] S. Liu, J. Shi, J. Liang, and M.-H. Yang. Face parsing via recurrent propagation. In *BMVC*, 2017. 1, 8
- [41] S. Liu, J. Yang, C. Huang, and M.-H. Yang. Multi-objective convolutional learning for face labeling. In *CVPR*, pages 3451–3459, 2015. 1, 2, 5, 7, 8
- [42] J. Long, E. Shelhamer, and T. Darrell. Fully convolutional networks for semantic segmentation. In *CVPR*, pages 3431–3440, 2015. 1, 2
- [43] P. Luc, C. Couprie, S. Chintala, and J. Verbeek. Semantic segmentation using adversarial networks. In *NIPS Workshop on Adversarial Training*, 2016. 2
- [44] X. Mao, Q. Li, H. Xie, R. Lau, and Z. Wang. Multi-class generative adversarial networks with the l2 loss function. *arXiv preprint arXiv:1611.04076*, 2016. 8
- [45] I. Masi, C. Ferrari, A. Del Bimbo, and G. Medioni. Pose independent face recognition by localizing local binary patterns via deformation components. In *ICPR*, 2014. 2, 3
- [46] J. Mathai, I. Masi, and W. Abd-Almageed. Does generative face completion help face recognition? In *ICB*, 2019. 1
- [47] R. Mohan and R. Nevatia. Using perceptual organization to extract 3d structures. *TPAMI*, (11):1121–1139, 1989. 2
- [48] Y. Nirkin, Y. Keller, and T. Hassner. FSGAN: Subject agnostic face swapping and reenactment. In *ICCV*, 2019. 1
- [49] Y. Nirkin, I. Masi, A. Tran, T. Hassner, and G. Medioni. On face segmentation, face swapping, and face perception. In *AFGR*, 2018. 1, 2, 3, 4, 7, 10, 11
- [50] S. Nowozin, C. H. Lampert, et al. Structured learning and prediction in computer vision. *Foundations and Trends® in Computer Graphics and Vision*, 6(3–4):185–365, 2011. 2
- [51] P. Pan, Y. Yan, T. Yang, and Y. Yang. Learning discriminators as energy networks in adversarial learning. *arXiv preprint arXiv:1810.01152*, 2018. 1, 8
- [52] O. M. Parkhi, A. Vedaldi, and A. Zisserman. Deep face recognition. In *BMVC*, 2015. 3
- [53] A. Paszke, S. Gross, S. Chintala, G. Chanan, E. Yang, Z. DeVito, Z. Lin, A. Desmaison, L. Antiga, and A. Lerer. Automatic differentiation in pytorch. In *NIPS Workshops*, 2017. 10
- [54] C. Peng, X. Zhang, G. Yu, G. Luo, and J. Sun. Large kernel matters—improve semantic segmentation by global convolutional network. In *CVPR*, pages 4353–4361, 2017. 1, 2
- [55] P. Z. Ramirez, A. Tonioni, and L. Di Stefano. Exploiting semantics in adversarial training for image-level domain adaptation. In *IPAS*, 2018. 2
- [56] O. Ronneberger, P. Fischer, and T. Brox. U-net: Convolutional networks for biomedical image segmentation. In *MICCAI*, pages 234–241, 2015. 3, 9
- [57] S. Ross, D. Munoz, M. Hebert, and J. A. Bagnell. Learning message-passing inference machines for structured prediction. In *CVPR*, 2011. 2
- [58] S. Saito, T. Li, and H. Li. Real-time facial segmentation and performance capture from rgb input. In *ECCV*, pages 244–261, 2016. 1, 2, 3, 4, 7
- [59] S. Sarkar and K. L. Boyer. Perceptual organization in computer vision: A review and a proposal for a classificatory structure. *TPAMI*, 23(2):382–399, 1993. 2
- [60] S. Saxena and J. Verbeek. Convolutional neural fabrics. In *NIPS*, 2016. 8
- [61] W. Shi, J. Caballero, F. Huszar, J. Totz, A. P. Aitken, R. Bishop, D. Rueckert, and Z. Wang. Real-time single image and video super-resolution using an efficient sub-pixel convolutional neural network. In *CVPR*, 2016. 4
- [62] Z. Shu, E. Yumer, S. Hadap, K. Sunkavalli, E. Shechtman, and D. Samaras. Neural face editing with intrinsic image disentanglement. In *CVPR*, pages 5541–5550, 2017. 1
- [63] M. Szummer, P. Kohli, and D. Hoiem. Learning crfs using graph cuts. In *ECCV*, 2008. 2, 5
- [64] S. Tsogkas, I. Kokkinos, G. Papandreou, and A. Vedaldi. Deep learning for semantic part segmentation with high-level guidance. *arXiv preprint arXiv:1505.02438*, 2015. 1, 8
- [65] S. Tulsiani, H. Su, L. J. Guibas, A. A. Efros, and J. Malik. Learning shape abstractions by assembling volumetric primitives. In *CVPR*, 2017. 2
- [66] Y. Wang, B. Luo, J. Shen, and M. Pantic. Face mask extraction in video sequence. *IJCV*, pages 1–17, 2018. 2
- [67] H. Yang, X. He, X. Jia, and I. Patras. Robust face alignment under occlusion via regional predictive power estimation. *TIP*, 24(8):2393–2403, Aug 2015. 7
- [68] Z. Yang and R. Nevatia. A multi-scale cascade fully convolutional network face detector. In *ICPR*, pages 633–638, 2016. 6
- [69] D. Yi, Z. Lei, S. Liao, and S. Z. Li. Learning face representation from scratch. *arXiv preprint arXiv:1411.7923*, 2014. 3
- [70] F. Yu and V. Koltun. Multi-scale context aggregation by dilated convolutions. In *ICLR*, 2016. 2, 4
- [71] F. Yu, V. Koltun, and T. Funkhouser. Dilated residual networks. In *CVPR*, 2017. 2, 4
- [72] J. Zhao, M. Mathieu, and Y. LeCun. Energy-based generative adversarial network. In *ICLR*, 2016. 8
- [73] H. Zheng, Y. Liu, M. Ji, F. Wu, and L. Fang. Learning high-level prior with convolutional neural networks for semantic segmentation. *arXiv preprint arXiv:1511.06988*, 2015. 8
- [74] S. Zheng, S. Jayasumana, B. Romera-Paredes, V. Vineet, Z. Su, D. Du, C. Huang, and P. H. Torr. Conditional random fields as recurrent neural networks. In *ICCV*, 2015. 2, 5